

## PRECONDITIONED BI-CONJUGATE GRADIENT METHOD FOR RADIATIVE TRANSFER IN SPHERICAL MEDIA

L. S. ANUSHA<sup>1</sup>, K. N. NAGENDRA<sup>1</sup>, F. PALETOU<sup>2</sup>, AND L. LÉGER<sup>2</sup>

<sup>1</sup> Indian Institute of Astrophysics, Koramangala, Bangalore 560 034, India

<sup>2</sup> Laboratoire d’Astrophysique de Toulouse-Tarbes, Université de Toulouse, CNRS, 14 Ave. E. Belin, 31400 Toulouse, France  
Received 2009 June 16; accepted 2009 August 21; published 2009 September 24

### ABSTRACT

A robust numerical method called the Preconditioned Bi-Conjugate Gradient (Pre-BiCG) method is proposed for the solution of the radiative transfer equation in spherical geometry. A variant of this method called Stabilized Preconditioned Bi-Conjugate Gradient (Pre-BiCG-STAB) is also presented. These are iterative methods based on the construction of a set of bi-orthogonal vectors. The application of the Pre-BiCG method in some benchmark tests shows that the method is quite versatile, and can handle difficult problems that may arise in astrophysical radiative transfer theory.

*Key words:* line: formation – methods: numerical – radiative transfer – scattering

### 1. INTRODUCTION

The solution of the transfer equation in spherical geometry remains a classic problem even 75 years after the first attempts by Chandrasekhar (1934) and Kosirev (1934), who used the Eddington approximation. In later decades, more accurate methods were given (see Mihalas 1978; Peraiah 2002, for historical reviews). Hummer & Rybicki (1971) and Kunasz & Hummer (1973, 1974) developed a variable Eddington factor method, and computed the solution on rays of a constant impact parameter (tangents to the discrete shells and parallel to the line of sight) in one-dimensional spherical geometry. This is a very efficient differential equation based technique which uses the Feautrier solution along rays of the constant impact parameter. An integral equation method was developed by Schmid-Burgk (1974) to solve the problem, again based on the tangent rays approach. Peraiah & Grant (1973) presented a highly accurate finite difference method based on the first-order form of the transfer equation. All these methods were later extended to expanding, and highly extended atmospheres. However, in this paper we confine our attention to static, one-dimensional spherical atmospheres.

In a next epoch in the development of spherical radiative transfer, the integral operator techniques were proposed. The idea of operator splitting and the use of approximate operators in iterative methods was brought to the astrophysical radiative transfer in planar media by Cannon (1973). Scharmer (1981) extended his work with a new definition of the approximate operator. The application of the integral operator technique to the spherical transfer started with the work of Hamann (1985) and Werner & Husfeld (1985). They used approximate operators that are diagonal, constructed from the core saturation approach. The  $\hat{A}$  operator contains the non-local coupling between all the spatial points. Olson et al. (1986) showed that the diagonal part (local coupling) of the actual  $\hat{A}$  operator itself is an optimum choice for the “approximate operator.” These methods are known as approximate Lambda Iteration (ALI) methods. The ALI methods, which are based on the concept of operator splitting and the use of the Jacobi iterative technique, were widely used in the later decades in radiative transfer theory (see Hubeny 2003; Hamann 2003, for historical reviews).

Gros et al. (1997) used an implicit integral method to solve static spherical line transfer problems. The most recent and interesting work on spherical radiative transfer is the papers by Asensio Ramos & Trujillo Bueno (2006) and Daniel & Cernicharo (2008), both of which are based on Gauss–Seidel (GS) and Successive Over Relaxation (SOR) iterative techniques.

Klein et al. (1989) were the first to use the BiCG technique in astrophysics. They use BiCG with an incomplete LU decomposition technique in their double splitting iterative scheme along with Orthomin acceleration. They applied it to a multi-dimensional line transfer problem. Auer (1991) describes a variant of Orthomin acceleration which uses “Minimization with respect to a set of Conjugate vectors.” He uses a set of  $n$  (usually  $n = 2$  or  $n = 4$ ) conjugate direction vectors which are orthogonal to each other, constructed using the residual vectors with a purpose to accelerate the convergence sequence.

Hubeny & Burrows (2007) developed GMRES (actually its variant called generalized conjugate residuals, GCR) method to solve the spherical transfer problem. It is based on an application of the idea of Krylov subspace techniques. They applied it to a more general time-dependent transport with velocity fields in a medium which scatters anisotropically. They apply the GMRES method to the neutrino transfer. It can also be used for the radiation transfer problem, including the simple problem of two-level atom line transfer discussed in this paper.

The Preconditioned Bi-Conjugate Gradient method (hereafter Pre-BiCG; see, e.g., Saad 2000) was first introduced to the line transfer in planar media by Paletou & Anterrieu (2009), who describe the method and compare it with other prevalent iterative methods, namely GS/SOR. In this paper, we adopt the Pre-BiCG method to the case of spherical media. We also show that the “Stabilized Preconditioned Bi-Conjugate Gradient (Pre-BiCG-STAB)” is even more advantageous in terms of memory requirements but with similar convergence rate as the Pre-BiCG method.

It is well known that the spherical radiative transfer in highly extended systems, despite being a straightforward problem, has two inherent numerical difficulties namely (1) peaking of the radiation field toward the radial direction, and (2) the  $(1/r^2)$  dilution of radiation in spherical geometry. To handle these, it becomes essential to take a very large number of angle ( $\mu$ ) points

**Table 1**The Sensitivity of Different Iterative Methods to the Convergence Criteria  $\bar{\omega}$ 

(a) $\bar{\omega} = 10^{-6}$					
$[N_{\text{pts}}/D]$	Jacobi	GS	SOR	Pre-BiCG	Pre-BiCG-STAB
5	81	40	24	16	12
8	136	69	22	19	15
30	444	230	74	33	23
(b) $\bar{\omega} = 10^{-8}$					
5	110	54	30	18	13
8	186	94	30	22	15
30	635	325	103	39	30
(c) $\bar{\omega} = 10^{-10}$					
5	138	68	37	20	14
8	236	118	40	25	18
30	827	419	132	45	30

**Notes.** Parts (a)–(c) correspond, respectively, to  $\bar{\omega} = 10^{-6}$ ,  $10^{-8}$ , and  $10^{-10}$ . Number of points per decade in the logarithmic  $\tau$  scale is denoted by  $[N_{\text{pts}}/D]$ . The SOR parameter used is 1.5. The entries under each method indicate the number of iterations required for convergence.

and spatial ( $\tau$ ) points, respectively. The existing ALI methods clearly slow down when extreme angular and spatial resolutions are demanded (for example, see Table 1). Therefore, there is a need to look for a method that is as efficient as ALI methods, but faster, and is relatively less sensitive to the grid resolution. The Pre-BiCG method and a variant of it provide such an alternative as we show in this paper.

Governing equations are presented in Section 2.1. In Section 2.2, we define the geometry of the problem and the specific details of gridding. In Section 2.3, the benchmark models are defined. We briefly recall the Jacobi and GS/SOR methods in Section 2.4. In Section 3, we describe the Pre-BiCG method. The computing algorithm is presented in Section 3.1. In Section 4, we describe the Pre-BiCG-STAB method briefly, and we give the computing algorithm in Section 4.1. In Section 5, we compare the performance of Pre-BiCG with the Jacobi, and GS/SOR methods. In Section 6, we validate this new method, by comparing with the existing well-known benchmark solutions in spherical line radiative transfer theory. Conclusions are presented in Section 7.

## 2. RADIATIVE TRANSFER IN A SPHERICAL MEDIUM

### 2.1. The Transfer Equation

In this paper, we restrict ourselves to the case of a two-level atom model. Further, we assume complete frequency redistribution (CRD). The transfer equation in a divergence form is written as

$$\mu \frac{\partial \mathbf{I}(r, \mu, x)}{\partial r} + \frac{1 - \mu^2}{r} \frac{\partial \mathbf{I}(r, \mu, x)}{\partial \mu} = [\chi_L(r)\phi(x) + \chi_C(r)] \times [\mathbf{S}(x, r) - \mathbf{I}(r, \mu, x)]. \quad (1)$$

Here  $\mathbf{I}$  is the specific intensity of radiation,  $\mathbf{S}$  is the source function,  $r$  is the radial distance,  $\mu$  is the direction cosine,  $x$  is the frequency measured in Doppler width units from the line center,  $\phi(x)$  is the line profile function, and  $\chi_L(r)$ ,  $\chi_C(r)$  are the line center and continuum opacities, respectively. The differential optical depth element is given by

$$d\tau(r) = -\chi_L(r)dr. \quad (2)$$

There are several methods which use the above form of the transfer equation (see Peraiah 2002). In our paper, we solve the transfer equation on a set of rays tangent to the spherical shells. It is written as

$$\pm \frac{\partial \mathbf{I}^\pm(z, p, x)}{\partial z} = [\chi_L(r)\phi(x) + \chi_C(r)] \times [\mathbf{S}(x, r) - \mathbf{I}^\pm(z, p, x)], \quad (3)$$

for the outgoing (+) and incoming (–) rays, respectively. Here  $z$  is the distance along the tangent rays and  $p$  is the distance from the center to the points on the vertical axis (the mid-line), where the tangent rays intersect it (see Figure 1). The direction cosines  $\mu$  ( $0 \leq \mu \leq 1$ ) are related to  $p$  by  $\mu = \sqrt{1 - (p^2/r^2)}$  for a shell of radius  $r$ . The optical depth scale along the tangent rays is now computed using  $d\tau(z) = d\tau(r)/\mu$ . In practical work, due to the symmetry of the problem, it is sufficient to perform the computations on a quadrant only. The source function is defined as

$$\mathbf{S}(x, r) = \frac{\chi_L(r)\phi(x)\mathbf{S}_L(r) + \chi_C(r)\mathbf{S}_C(r)}{\chi_L(r)\phi(x) + \chi_C(r)}. \quad (4)$$

$\mathbf{S}_C(r)$  is the continuum source function taken as the Planck function  $\mathbf{B}_\nu(r)$  throughout this paper. The monochromatic optical depth scale  $\Delta\tau_x = \Delta\tau_z[\phi(x) + \beta_c]$ , with  $\beta_c = \chi_C(r)/\chi_L(r)$  along the tangent rays. For simplicity, hereafter we omit the subscript  $z$  from  $\tau_z$  and write  $\tau$  to denote  $\tau_z$ . The line source function is given by

$$\mathbf{S}_L(r) = (1 - \epsilon) \int_{-1}^1 \frac{d\mu'}{2} \int_{-\infty}^{\infty} dx' \phi(x') \mathbf{I}(\tau, \mu', x') + \epsilon \mathbf{B}_\nu(r), \quad (5)$$

with the thermalization parameter defined in the conventional manner as  $\epsilon = C_{\text{ul}}/(A_{\text{ul}} + C_{\text{ul}})$ , where  $C_{\text{ul}}$  and  $A_{\text{ul}}$  are collisional and radiative de-excitation rates. The intensity along the rays is computed using the formal solution integral

$$\mathbf{I}^+(\tau, p, x) = \mathbf{I}_0^+(\tau, p, x) \exp[-\Delta\tau_x] + \int_{\tau}^T \exp[-\Delta\tau'_x] \mathbf{S}(\tau') [\phi(x) + \beta_c] d\tau'. \quad (6)$$

The corresponding integral for the incoming rays is

$$\mathbf{I}^-(\tau, p, x) = \mathbf{I}_0^-(\tau, p, x) \exp[-\Delta\tau_x] + \int_0^{\tau} \exp[-\Delta\tau'_x] \mathbf{S}(\tau') [\phi(x) + \beta_c] d\tau'. \quad (7)$$

Here,  $\mathbf{I}_0^+(\tau, p, x)$  represents the inner boundary condition imposed on the core and along the mid-vertical line (see Figure 1).  $\mathbf{I}_0^-(\tau, p, x)$  is the outer boundary condition specified at the surface of the spherical atmosphere. When the above formal integral is applied to a stencil of short characteristic (MOP) along a tangent ray, it takes a simple algebraic form,

$$\mathbf{I}^\pm(\tau, p, x) = \mathbf{I}_O^\pm(\tau, p, x) \exp[-\Delta\tau_M] + \Psi_M^\pm(\tau, p, x) \mathbf{S}_M + \Psi_O^\pm(\tau, p, x) \mathbf{S}_O + \Psi_P^\pm(\tau, p, x) \mathbf{S}_P, \quad (8)$$

where  $\mathbf{S}_{M,O,P}$  are the source function values at M, O, and P points on a short characteristic. The coefficients  $\Psi$  are calculated following the method described in Kunasz & Auer (1988).



2.4. Iterative Methods of ALI Type for a Spherical Medium

The ALI methods have been successfully used for the solution of the transfer equation in spherical shell atmospheres (see, e.g., Hamann 2003, and references therein). These authors use the Jacobi iterative methods (first introduced by Olson et al. 1986) for computing the source function corrections. Recently, the GS method has been proposed to solve the same problem (see, e.g., Asensio Ramos & Trujillo Bueno 2006; Daniel & Cernicharo 2008). Hubeny & Burrows (2007) proposed the GMRES method for solving the spherical radiative transfer problem. GMRES and Pre-BiCG both belong to the Krylov subspace technique. In this paper, we compute the spherical transfer solutions by the Jacobi and GS/SOR methods, and compare with the solutions computed using the Pre-BiCG method. For the sake of clarity, we recall briefly the steps of the Jacobi and GS/SOR methods. *Jacobi iteration cycle.* The source function corrections are given by

$$\delta S_k^n = S_k^{n+1} - S_k^n = \frac{(1 - \epsilon)\bar{J}_k^n + \epsilon B_v - S_k^n}{[1 - (1 - \epsilon)\hat{\Lambda}_{k,k}^*]}, \quad (15)$$

for the  $n$ th iterate. Here  $k$  is the depth index.  $\hat{\Lambda}^*$  is the approximate operator which is simply taken as the diagonal of the actual  $\hat{\Lambda}$  operator defined through

$$\hat{\Lambda}[S] = \bar{J}, \quad (16)$$

$$\bar{J}(\tau) = \int_{-1}^{+1} \frac{d\mu'}{2} \int_{-\infty}^{\infty} dx' \phi(x') I(\tau, \mu', x'). \quad (17)$$

*GS/SOR iteration cycle.* The essential difference between the Jacobi and GS/SOR methods is the following:

$$S_k^{n+1} = S_k^n + \omega \delta S_k^n. \quad (18)$$

Here, the parameter  $\omega$  is called the relaxation parameter which is unity for the GS technique.

The SOR method is derived from the GS method by simply taking  $1 < \omega < 2$  (see Trujillo Bueno & Fabiani Bendicho 1995, for details). The source function correction for the GS method is given by

$$\delta S_k^n = \frac{(1 - \epsilon)\bar{J}_k^{n(\text{old+new})} + \epsilon B_v - S_k^n}{[1 - (1 - \epsilon)\hat{\Lambda}_{k,k}^*]}, \quad (19)$$

where the quantity  $\bar{J}_k^{n(\text{old+new})}$  denotes the mean intensity computed using new values of the source function as soon as they become available. For those depth points for which the source function correction is not yet complete, the GS method uses the values of the source function corresponding to the previous iteration (see Trujillo Bueno & Fabiani Bendicho 1995). For clarity, we explain how the GS algorithm works in spherical geometry, on rays of the constant impact parameter:

- Begin loop over iterations
- Begin loop over radial shells with index  $k$
- Begin loop over impact parameters (or directions) with increasing  $p$
- For the  $n$ th iteration:

**For the incoming rays ( $\mu < 0$ ):**  
**(Reverse sweep along radial shells)**

1. This part of the calculations starts at the outer boundary for all impact parameter rays.
2.  $I_k$  are first calculated for a given radial shell  $k$  using  $S_k^n$ ,  $S_{k-1}^n$ , and  $S_{k+1}^n$ .
3. The partial integral  $\bar{J}_k(\mu < 0)$  are calculated before proceeding to the next shell. This part of the calculations is stopped when the core (for the core rays) and the mid-vertical line (for the lobe rays) are reached.

**For outgoing rays ( $\mu > 0$ ):**  
**(Forward sweep along radial shells)**

4. This part of the calculations starts at the inner boundary. First, for the radial shell with  $k = N_d$   $\bar{J}_{N_d}$  is calculated, using boundary conditions  $I_{N_d}$ .
5.  $\delta S_{N_d}^n$  is computed and the source function is updated using  $S_{N_d}^{n+1} = S_{N_d}^n + \delta S_{N_d}^n$ .
6. For the next radial shell  $k = N_d - 1$ : to calculate  $I_{N_d-1}$  by applying the short characteristic formula,  $S_{N_d}$ ,  $S_{N_d-1}$  and  $S_{N_d-2}$  are needed. Already  $S_{N_d}^{n+1}$ ,  $S_{N_d-1}^n$  and  $S_{N_d-2}^n$  are available. GS takes advantage of the available new source function at  $k = N_d$ .  $I_{N_d-1}$  is calculated with this set of source functions.
7. Then  $\bar{J}_{N_d-1}(\mu > 0)$  are calculated using  $I_{N_d-1}$ .
8. Note that,  $\bar{J}_{N_d-1}(\mu < 0)$  was calculated using  $S_{N_d}^n$ ,  $S_{N_d-1}^n$ , and  $S_{N_d-2}^n$  whereas  $\bar{J}_{N_d-1}(\mu > 0)$  used the “updated” source function  $S_{N_d}^{n+1}$ . Therefore,  $\bar{J}_{N_d-1}$  is corrected by adding the following correction:

$$\Delta \bar{J}_{N_d-1} = \delta S_{N_d}^{n+1} \int_{-1}^0 \Psi_{N_d}(\mu < 0) d\mu.$$

9.  $\delta S_{N_d-1}^n$  and  $S_{N_d-1}^{n+1} = S_{N_d-1}^n + \delta S_{N_d-1}^n$  are now calculated.
10. Since “updated”  $S_{N_d-1}^{n+1}$  at  $k = N_d - 1$  is also available now, before going to the next radial shell it is appropriate to correct the intensity at the present radial shell by adding to it, the following correction term

$$\Delta I_{N_d-1}(\mu) = \delta S_{N_d-1}^{n+1} \Psi_{N_d-1}.$$

- End loop over impact parameters (or directions)
- End loop over radial shells
- End loop over iterations.

3. PRECONDITIONED BiCG METHOD FOR A SPHERICAL MEDIUM

In this section, we first describe the essential ideas of the Pre-BiCG method. The complete theory of the method is described in Saad (2000). We recall that the two-level atom source function with a background continuum is given by

$$S(x, r) = \frac{\chi_L(r)\phi(x)S_L(r) + \chi_C(r)S_C(r)}{\chi_L(r)\phi(x) + \chi_C(r)}. \quad (20)$$

It can be re-written as

$$S(x, r) = \tilde{p}(x, r)S_L(r) + (1 - \tilde{p}(x, r))S_C(r), \quad (21)$$

where

$$\tilde{p}(x, r) = \frac{\chi_L(r)\phi(x)}{\chi_L(r)\phi(x) + \chi_C(r)}. \quad (22)$$

From Equations (5), (16), and (17), we obtain

$$S(x, r) = \tilde{p}(x, r)\{(1 - \epsilon)\hat{\Lambda}[S(x, r)] + \epsilon \mathbf{B}_v(r)\} + (1 - \tilde{p}(x, r))S_c(r). \quad (23)$$

Therefore, the system of equations to be solved becomes

$$[\hat{I} - (1 - \epsilon)\tilde{p}(x, r)\hat{\Lambda}]S(x, r) = \tilde{p}(x, r)\epsilon \mathbf{B}_v(r) + (1 - \tilde{p}(x, r))S_c(r), \quad (24)$$

which can be expressed in a symbolic form as

$$\hat{A}\mathbf{y} = \mathbf{b}, \quad \text{with} \\ \hat{A} = [\hat{I} - (1 - \epsilon)\tilde{p}(x, r)\hat{\Lambda}]; \quad \mathbf{y} = S(x, r). \quad (25)$$

The vector  $\mathbf{b}$  represents quantities on the right-hand side of Equation (24). Now we describe briefly, how the Pre-BiCG method differs from ALI-based methods.

Let  $\mathbb{R}^n$  denote the  $n$ -dimensional Euclidean space of real numbers.

*Definition.* The Pre-BiCG algorithm is a process involving projections onto the  $m$ -dimensional subspace ( $m \leq n$ ) of  $\mathbb{R}^n$ ,

$$\mathcal{K}_m = \text{span}\{\mathbf{v}_1, \hat{A}\mathbf{v}_1, \dots, \hat{A}^{m-1}\mathbf{v}_1\}, \quad (26)$$

and also being orthogonal to another  $m$ -dimensional subspace of  $\mathbb{R}^n$ ,

$$\mathcal{L}_m = \text{span}\{\mathbf{w}_1, \hat{A}^T\mathbf{w}_1, \dots, \hat{A}^{T(m-1)}\mathbf{w}_1\}. \quad (27)$$

Here  $\mathbf{v}_1$  is taken as the initial residual vector  $\mathbf{r}_0 = \mathbf{b} - \hat{A}\mathbf{y}_0$  with  $\mathbf{y}_0$  being the initial guess for the solution of Equation (25). The vector  $\mathbf{w}_1$  is taken as arbitrary such that the inner product  $\langle \mathbf{v}_1, \mathbf{w}_1 \rangle \neq 0$ . The method recursively constructs a pair of bi-orthogonal bases  $\{\mathbf{v}_i; i = 1, 2, \dots, m\}$  and  $\{\mathbf{w}_i; i = 1, 2, \dots, m\}$  for  $\mathcal{K}_m$  and  $\mathcal{L}_m$ , respectively, such that they satisfy the bi-orthogonality condition  $\langle \mathbf{v}_i, \mathbf{w}_j \rangle = \delta_{ij}$ . For the purpose of application to the radiative transfer theory, it is convenient to write the Pre-BiCG steps in the form of an algorithm. For simplicity we drop the explicit dependence on variables.

### 3.1. The Preconditioned BiCG Algorithm

Our goal is to solve Equation (25). In this section, the symbols  $\mathbf{r}_i$  and  $\mathbf{p}_i$  are used to be in conformity with the standard notation of residual and conjugate direction vectors. They should not be confused with the radius vector  $r_i$  and impact parameter  $p_i$  which appear in spherical radiative transfer theory.

1. The very first step is to construct and store the matrix  $\hat{A}^T$  (which does not change with iterations, for the cases considered here, namely the two-level atom model).

Details of computing  $\hat{A}^T$  efficiently is described in the [Appendix](#).

We follow the preconditioned version of the BiCG method. Preconditioning is a process in which the original system of equations is transformed into a new system, which has a faster rate of convergence. For example, this can be done by solving the new system  $\hat{M}^{-1}\hat{A}\mathbf{y} = \hat{M}^{-1}\mathbf{b}$  where  $\hat{M}$  is an appropriately chosen matrix, called the ‘‘preconditioner’’ (see also Equation (2) of Auer 1991). This preconditioner is chosen in such a way that

- a) the new system should be easier to solve,

- b)  $\hat{M}^{-1}$  itself should be inexpensive to operate on an arbitrary vector,
- c) the preconditioning is expected to increase the convergence rate.

The choice of the preconditioner depends on the problem at hand. When an appropriate  $\hat{\Lambda}^*$  is chosen such that the amplification matrix  $[\hat{I} - (1 - \epsilon)\hat{\Lambda}^*]$  has as small a maximum eigenvalue as possible (see Olson et al. 1986), the convergence rate is enhanced. What enables the convergence of ALI, which satisfies the above property, and simplest to manipulate, is the diagonal of  $\hat{\Lambda}$  itself. Therefore, the amplification matrix  $[\hat{I} - (1 - \epsilon)\hat{\Lambda}^*]$  with a diagonal form for  $\hat{\Lambda}^*$  is a simple and natural choice as a ‘‘preconditioner.’’ We construct the preconditioner matrix  $\hat{M}$  by taking it as the diagonal of  $\hat{A}$ .

2. An initial guess for the source function is

$$\mathbf{y}_0 = \tilde{p}\epsilon \mathbf{B} + (1 - \tilde{p})S_c, \quad (28)$$

where the thermal part  $\epsilon \mathbf{B}$  is taken as an initial guess for  $S_L$ .

3. The formal solver is used with  $\mathbf{y}_0$  as input to calculate  $\tilde{\mathbf{J}}(\mathbf{y}_0)$ .
4. The initial residual vector is computed using

$$\mathbf{r}_0 = \mathbf{b} - \hat{A}\mathbf{y}_0. \quad (29)$$

5. The initial bi-orthogonal counterpart  $\mathbf{r}_0^*$  for  $\mathbf{r}_0$  is chosen such that we have  $\langle \mathbf{r}_0, \mathbf{r}_0^* \rangle \neq 0$ . One can choose  $\mathbf{r}_0^* = \mathbf{r}_0$  oneself.

Such an initial choice of  $\mathbf{r}_0^*$  vector is necessary, as the method is based on the construction of bi-orthogonal residual vectors  $\mathbf{r}_i$  and  $\mathbf{r}_i^*$  recursively, for  $i = 1, 2, \dots, m$ , where  $m$  is the number of iterations required for convergence. The process of constructing the bi-orthogonal vectors gets completed, once we reach the convergence. In other words, the number of bi-orthogonal vectors necessary to guarantee a converged solution represents the actual number of iterations itself. It is useful to remember that when we refer to ‘‘bi-orthogonality’’ hereafter, say, e.g., of the residual vectors  $\mathbf{r}_i, \mathbf{r}_i^*$ , we simply mean that  $\langle \mathbf{r}_i, \mathbf{r}_j^* \rangle = 0$  for  $i \neq j$ , but  $\langle \mathbf{r}_i, \mathbf{r}_i^* \rangle$  need not be unity.

6. The bi-orthogonalization process makes use of conjugate direction vectors  $\mathbf{p}$  and  $\mathbf{p}^*$  for each iteration. They can be constructed during the iterative process, again through recursive relations. An initial guess to these vectors is made as  $\mathbf{p}_0 = \mathbf{r}_0$  and  $\mathbf{p}_0^* = \mathbf{r}_0^*$ .
7. The preconditioned initial residual vectors  $\boldsymbol{\zeta}_0^*$  are computed using

$$\boldsymbol{\zeta}_0^* = \hat{M}^{-1}\mathbf{r}_0^*. \quad (30)$$

8. For  $i = 1, 2, \dots$ , the following steps are carried out until convergence.
9. Using the formal solver with  $\mathbf{p}_i$  as input (instead of the actual source vector  $\mathbf{y}$ ),  $\tilde{\mathbf{J}}[\mathbf{p}_i]$  is obtained.
10.  $\hat{A}[\mathbf{p}_i]$  is computed using

$$\hat{A}[\mathbf{p}_i] = \mathbf{p}_i - (1 - \epsilon)\tilde{p}\tilde{\mathbf{J}}[\mathbf{p}_i]. \quad (31)$$

11. The inner products

$$\langle \hat{A}[\mathbf{p}_i], \mathbf{p}_i^* \rangle \quad \text{and} \quad \langle \mathbf{r}_i, \boldsymbol{\zeta}_i^* \rangle \quad (32)$$

are computed and used to estimate the quantity

$$\alpha_i = \frac{\langle \mathbf{r}_i, \boldsymbol{\zeta}_i^* \rangle}{\langle \hat{A}[\mathbf{p}_i], \mathbf{p}_i^* \rangle}. \tag{33}$$

12. The new source function is obtained through

$$\mathbf{y}_{i+1} = \mathbf{y}_i + \alpha_i \mathbf{p}_i. \tag{34}$$

*Test for Convergence.* Let  $\bar{\omega}$  denote the convergence criteria. If

$$\max_{\tau} \{\delta \mathbf{y} / \mathbf{y}\} \leq \bar{\omega}, \tag{35}$$

then the iteration sequence is terminated. Otherwise it is continued from step (13) onward. The convergence criteria  $\bar{\omega}$  are chosen depending on the problem.

13. Following recursive relations are used to compute the new set of vectors to be used in the  $(i + 1)$ th iteration:

$$\mathbf{r}_{i+1} = \mathbf{r}_i - \alpha_i \hat{A}[\mathbf{p}_i], \tag{36}$$

$$\mathbf{r}_{i+1}^* = \mathbf{r}_i^* - \alpha_i \hat{A}^T[\mathbf{p}_i^*], \tag{37}$$

$$\boldsymbol{\zeta}_{i+1}^* = \hat{M}^{-1} \mathbf{r}_{i+1}^*. \tag{38}$$

14. The quantity  $\beta_i$  is computed using

$$\beta_i = \frac{\langle \mathbf{r}_{i+1}, \boldsymbol{\zeta}_{i+1}^* \rangle}{\langle \mathbf{r}_i, \boldsymbol{\zeta}_i^* \rangle}. \tag{39}$$

15. The conjugate direction vectors for the  $(i + 1)$ th iteration are computed through

$$\begin{aligned} \mathbf{p}_{i+1} &= \mathbf{r}_{i+1} + \beta_i \mathbf{p}_i, \\ \mathbf{p}_{i+1}^* &= \mathbf{r}_{i+1}^* + \beta_i \mathbf{p}_i^*. \end{aligned} \tag{40}$$

16. The control is transferred to step (8).

The converged source function  $\mathbf{y}$  is finally used to compute the specific intensity everywhere within the spherical medium.

#### 4. TRANSPOSE FREE VARIANT: Pre-BiCG-STAB

In spite of higher convergence rate, computation and storage of the  $\hat{A}^T$  matrix are main disadvantages of the Pre-BiCG method. To avoid this, and to make use of only the “action” of  $\hat{A}$  matrix on an arbitrary vector, a method called “BiCG-squared” was developed (See Saad 2000, for references and details), which is based on squaring the residual polynomials. Later it was improved by re-defining the residual polynomial as a product of two polynomials and obtaining a recursive relation for the new residual polynomial. This product involves residual polynomial of the Pre-BiCG method and a new polynomial which “smoothen” the iterative process. In this section, we give the computing algorithm of the Pre-BiCG-STAB method as applied to a radiative transfer problem. As described below, we can avoid computing and storing of the  $\hat{A}^T$  matrix in the Pre-BiCG-STAB method. However, we would now need to call the formal solver twice per iteration unlike in the Pre-BiCG method, where it is called only once. This results in an increase in the number of operations per iteration when compared to the Pre-BiCG method, causing a slight increase in the CPU time per iteration. In spite of these, the Pre-BiCG-STAB method turns out to be always faster than the regular Pre-BiCG method in terms of convergence rate (lesser number of iterations for convergence).

#### 4.1. Pre-BiCG-STAB Algorithm

Now we give the algorithm of the Pre-BiCG-STAB method to solve the system  $\hat{M}^{-1} \hat{A} \mathbf{S} = \hat{M}^{-1} \mathbf{b}$ . Here  $\hat{M}$  is a suitably chosen preconditioner matrix. The computing algorithm is organized as follows.

1. First initial preconditioned residual vectors and conjugate direction vectors are defined through

$$\mathbf{z}_0 = \hat{M}^{-1} \mathbf{b} - \hat{M}^{-1} \hat{A} \mathbf{S}, \tag{41}$$

$$\mathbf{z}_0^* = \mathbf{z}_0, \quad \mathbf{P}_0 = \mathbf{z}_0. \tag{42}$$

2. For  $j = 1, 2, \dots$ , the following steps are carried out until convergence.

3. Using  $\mathbf{P}_j$  instead of the source function a call to the formal solver is made to compute  $\hat{A} \mathbf{P}_j$ .

4. The coefficient  $\alpha_j$  can be evaluated now as

$$\alpha_j = \frac{\langle \mathbf{z}_j, \mathbf{z}_0^* \rangle}{\langle \hat{M}^{-1} \hat{A} \mathbf{P}_j, \mathbf{z}_0^* \rangle}. \tag{43}$$

5. Another vector  $\mathbf{q}_j$  is calculated as

$$\mathbf{q}_j = \mathbf{z}_j - \alpha_j \hat{M}^{-1} \hat{A} \mathbf{P}_j. \tag{44}$$

6. Using  $\mathbf{q}_j$  in place of the source function a call to the formal solver is made to obtain  $\hat{A} \mathbf{q}_j$ .

7. The coefficient  $\omega_j$  is estimated as

$$\omega_j = \frac{\langle \hat{M}^{-1} \hat{A} \mathbf{q}_j, \mathbf{q}_j \rangle}{\langle \hat{M}^{-1} \hat{A} \mathbf{q}_j, \hat{M}^{-1} \hat{A} \mathbf{q}_j \rangle}. \tag{45}$$

8. The updated new source function is calculated as

$$\mathbf{S}_{j+1} = \mathbf{S}_j + \alpha_j \mathbf{P}_j + \omega_j \mathbf{q}_j. \tag{46}$$

9. Test for convergence is made as in the Pre-BiCG algorithm.

10. Before going to the next iteration a set of recursive relations are used to compute residual vectors

$$\mathbf{z}_{j+1} = \mathbf{q}_j - \omega_j \hat{M}^{-1} \hat{A} \mathbf{q}_j, \tag{47}$$

and conjugate direction vectors

$$\mathbf{P}_{j+1} = \mathbf{z}_{j+1} + \beta_j (\mathbf{P}_j - \omega_j \hat{M}^{-1} \hat{A} \mathbf{P}_j). \tag{48}$$

for the next iteration, where the coefficient  $\beta_j$  is

$$\beta_j = \frac{\langle \mathbf{z}_{j+1}, \mathbf{z}_0^* \rangle}{\langle \mathbf{z}_j, \mathbf{z}_0^* \rangle} \frac{\alpha_j}{\omega_j}. \tag{49}$$

11. The control is now transferred to step (2).

#### 5. COMPARISON OF ALI AND Pre-BiCG METHODS

There are two characteristic quantities that define iterative techniques. They are (1) convergence rate, which is nothing but the maximum relative change (MRC) defined as

$$R_c = \max_{\tau} \left\{ \frac{\delta S^n}{S^n} \right\}, \tag{50}$$

and (2) the total CPU time  $T_{\text{total}}$  required for convergence.  $T_{\text{total}}$  is the time taken to reach a given level of convergence, taking account only of the arithmetic manipulations within the iteration cycle. We also define a quantity called the true error  $T_e$  and use it to evaluate these methods.

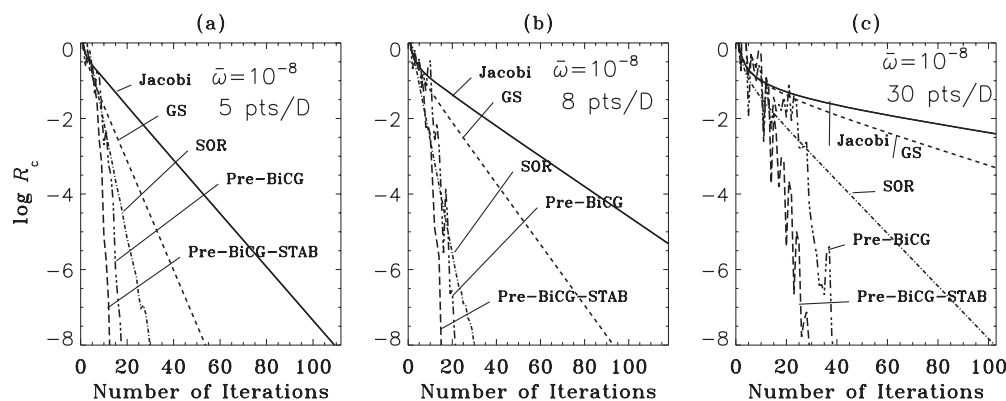


**Figure 2.** Dependence of the MRC  $R_c$  on the iterative progress for different methods. Panels (a)–(c) represent models with low, medium, and high spatial resolution, respectively. The model parameters are  $(\bar{n}, R, T, a, \epsilon, \beta_c, B_v) = (0, 10, 10^3, 10^{-3}, 10^{-4}, 0, 1)$ . The convergence criteria are chosen arbitrarily as  $\bar{\omega} = 10^{-8}$ . The SOR parameter  $\omega = 1.5$ . The figures show clearly that the Jacobi method has the smallest convergence rate, which progressively increases for the GS and SOR methods. The Pre-BiCG and Pre-BiCG-STAB methods generally have the largest convergence rate compared to the other three.

**Table 2**  
Timing Efficiency of the Iterative Methods

Quantity Compared	Jacobi	GS	SOR	Pre-BiCG	Pre-BiCG-STAB
CPU time for convergence	7 minutes 49 s	4 minutes 4 s	1 minute 18 s	27 s	42 sec
Overrates in computing	6 s	6 s	6 s	9 s	6 sec
Total computing time	7 minutes 55 s	4 minutes 10 s	1 minute 24 s	36 s	48 sec

### 5.1. The Behavior of the Maximum Relative Change (MRC)

In this section, we compare  $R_c$  and  $T_{\text{total}}$  for the Jacobi, GS, SOR, Pre-BiCG, and the Pre-BiCG-STAB methods. The SOR parameter used is 1.5. It is worth noting that the overrates (the time taken to prepare the necessary setup, before initiating the iterative cycle) are expected to be different for different methods. For instance, in Jacobi and GS/SOR this is essentially the CPU time required to set up the  $\hat{\Lambda}^*$  matrix. In the Pre-BiCG method, this involves the time taken to construct the  $\hat{A}^T$  matrix, which is a critical quantity of this method. The Pre-BiCG method is described in this paper in the context of a two-level atom model, because of which, we do not need to update the  $\hat{A}^T$  matrix at each iteration. For the Pre-BiCG-STAB method it is the time taken to construct the preconditioner matrix  $\hat{M}$ .

Figure 2 shows a plot of  $R_c$  for different methods. We can take  $R_c$  as a measure of the convergence rate. Chevallier et al. (2003) show that it always becomes necessary to use high-resolution grids, to achieve high accuracy of the solution (see also Section 1). This is especially true in the case of spherical radiative transfer where a spatial grid with a large number of points per decade becomes necessary to achieve reasonable accuracy. In the following, we discuss how different methods respond to the grid refinement. It is a well-known fact with the ALI methods that the convergence rate is small when the resolution of the depth grid is very high. In contrast, they have a high convergence rate in low-resolution grids. On the other hand,  $R_c$  of the Pre-BiCG and Pre-BiCG-STAB methods have higher convergence rate even in a high-resolution grid. Figure 2(a) shows  $R_c$  for different methods when a low-resolution spatial grid is used (5 pts/D in the logarithmic scale for the  $\tau$  grid). The Jacobi method has a low convergence rate. In comparison, GS has a convergence rate which is twice that of Jacobi. SOR has a rate that is even better than that of GS. However, the Pre-BiCG and Pre-BiCG-STAB methods have the higher convergence rate. Figures 2(b) and (c) are shown for intermediate (8 pts/D) and high (30 pts/D) grid resolutions. The essential point to note

is that, as the grid resolution increases, the convergence rate decreases drastically and monotonically for the Jacobi and the GS method. It is not so drastic for the SOR method which shows non-monotonic dependence on grid resolution. The Pre-BiCG and Pre-BiCG-STAB methods exhibit again a monotonic behavior apart from being relatively less sensitive to the grid resolution.

In Table 1, we show what happens when we set convergence criteria to progressively smaller values ( $\bar{\omega} = 10^{-6}$ ,  $10^{-8}$ , and  $10^{-10}$  for Tables 1(a)–(c), respectively) for various grid resolutions. The model used to compute these results is  $(\bar{n}, R, T, a, \epsilon, \beta_c, B_v) = (0, 10, 10^3, 10^{-3}, 10^{-4}, 0, 1)$ . The idea is to demonstrate that for a given grid resolution (corresponding rows of Tables 1(a)–(c), all the methods show a monotonic increase in the number of iterations for convergence, as we decrease  $\bar{\omega}$ . On the other hand, Pre-BiCG and Pre-BiCG-STAB require much less number of iterations to reach the same level of accuracy.

*CPU time considerations.* Table 2 shows the CPU time requirements for the methods discussed in this paper. The model used to compute these test cases is  $(\bar{n}, R, T, \epsilon, \beta_c, B_v, \bar{\omega}) = (0, 300, 10^3, 10^{-4}, 0, 1, 10^{-8})$ . The grid resolution considered is 30 pts/D. The CPU time for convergence can be defined as the computing time required to complete the convergence cycle and reach a fixed level of accuracy. We recall that the overrates in computing time is the time taken to prepare the necessary setup before initiating the iterative cycle. Total computing time is the sum of these two. In the Appendix, we discuss in detail how to construct the  $\hat{\Lambda}^*$  matrix for the Jacobi, GS/SOR methods and  $\hat{A}$  and  $\hat{M}$  matrices for the Pre-BiCG and Pre-BiCG-STAB methods, respectively, with an optimum effort. Construction of these matrices constitutes the overrates in computing time of each method. The first row of Table 2 shows that Pre-BiCG is the fastest to complete the convergence cycle. The reason why Pre-BiCG-STAB takes slightly longer time than Pre-BiCG is explained at the end of Section 4.

The second row of Table 2 shows that all methods except Pre-BiCG take nearly 8 s as overrates for the chosen model.

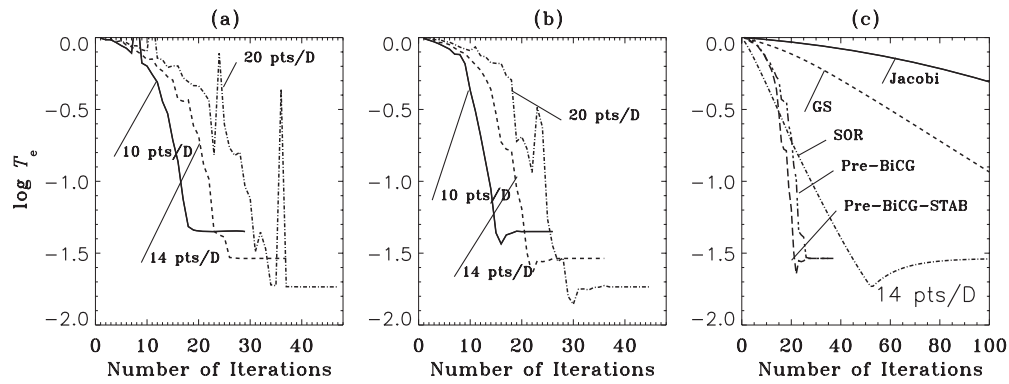


**Figure 3.** Behavior of the true error  $T_e$  in a spherically symmetric medium. The model parameters are  $(\tilde{n}, R, T, \epsilon, \beta_c, B_v) = (0, 10, 10^3, 10^{-4}, 0, 1)$ . Panel (a) shows the decrement of the true error of the Pre-BiCG method for three different spatial grid resolutions. Notice the plateau in the true error. Panel (b) shows  $T_e$  for the Pre-BiCG-STAB method. Panel (c) shows for different methods the number of iterations required to reach a constant true error  $2.9 \times 10^{-2}$ . The SOR parameter  $\omega = 1.5$ . The overall behavior of the curves is the same for all the methods, although the rates of decrement are different.

Pre-BiCG takes additional 3–4 s as explicit integrals are performed for computing off-diagonal elements also (unlike the other methods where such integrals are performed only for diagonal elements).

The last row of Table 2 shows that in terms of total CPU time requirements, the other methods fall behind Pre-BiCG and Pre-BiCG-STAB. Pre-BiCG seems to be a bit faster compared to Pre-BiCG-STAB for the particular model chosen. However, it is model dependent. For instance, as the contribution toward overrates increases, Pre-BiCG-STAB clearly stands out as the fastest method among all those discussed in this paper.

### 5.2. A Study of the True Error

We now study the true errors in these methods (see Figure 3). The model parameters are  $(\tilde{n}, R, T, \epsilon, \beta_c, B_v) = (0, 10, 10^3, 10^{-4}, 0, 1)$ . A coherent scattering limit is used. To define a true error, we need a so-called exact solution. Except for highly idealized cases, exact solutions do not exist. For practical purposes, the exact solution can be defined as a solution obtained on a spatial grid of resolution that is three times larger than the grid resolution of the model that we are interested in. Also, we extend the iteration until  $R_c$  reaches an extremely small value of  $10^{-12}$ . The source function computed in this way can be called  $S(\infty, \infty)$ , the fully converged solution on an infinite resolution (see Auer et al. 1994). The source function at the  $n$ th iterate is denoted by  $S^n$ . We define the true error as

$$T_e = \max_{\tau} \left| \frac{S^n - S_{\text{exact}}}{S_{\text{exact}}} \right|, \quad (51)$$

following Trujillo Bueno & Fabiani Bendicho (1995). In Figure 3(a), we show  $T_e$  computed for the Pre-BiCG method using three grid resolutions, namely 10 pts/D, 14 pts/D, and 20 pts/D. The plateau of each curve represents the minimum value of the true error reached for a given grid resolution. We notice that as the resolution increases,  $T_e$  gradually decreases in magnitude as expected. In Figure 3(b), we show  $T_e$  computed for the Pre-BiCG-STAB method. The model parameters are the same as in Figure 3(a). Clearly, Pre-BiCG-STAB shows a smooth decrement of the true error compared to Pre-BiCG, because of the smoothing polynomial used to define the residual vectors. In Figure 3(c), we compare the decrement of true errors for different iterative methods. The grid resolution chosen is 14 pts/D with other model parameters being the same as in Figures 3(a) and (b). The decrease of the true errors follows the same pattern in all the iterative methods, although the

number of iterations required for  $T_e$  to reach a constant value (plateau) depends on the method. To reach the same level of the true error, the Pre-BiCG and Pre-BiCG-STAB methods require considerably less number of iterations, when compared to the other three.

### 5.3. A Theoretical Upper Bound on the Number of Iterations for Convergence in the Pre-BiCG Method

Suppose that  $\hat{A}$  is an  $N_d \times N_d$  matrix. The solution to the problem  $\hat{A} \mathbf{y} = \mathbf{b}$  is a vector of length  $N_d$ . In an  $N_d$ -dimensional vector space,  $V_{N_d}$  the maximum number of linearly independent vectors is  $N_d$ . Hence, there can at the most be  $N_d$  orthogonal vectors in  $V_{N_d}$ . The Pre-BiCG method seeks a solution by constructing orthogonal vectors. We recall that the residual counterpart vectors  $\{\mathbf{r}_1^*, \mathbf{r}_2^*, \dots, \mathbf{r}_M^*\}$  constructed during the iteration process are orthogonal to the initial residual vector  $\mathbf{r}_0$ . Thus, when we reach convergence after  $M$  iterations, we will have a set of  $M+1$  orthogonal vectors  $\{\mathbf{r}_0, \mathbf{r}_1^*, \mathbf{r}_2^*, \dots, \mathbf{r}_M^*\}$ . From the arguments given above, it is clear that  $M+1 \leq N_d$ , namely in the Pre-BiCG method, “the convergence must be reached theoretically in at the most  $N_d$  steps (or iterations).” This sets an upper limit to the number of iterations to reach convergence (see also Hestenes & Stiefel 1952). For example, when the dimensionality of a problem is high (a very large value of  $N_d$ ), the Pre-BiCG method ensures convergence in at the most  $N_d$  iterations. A theoretical upper bound on the number of iterations also exists for the Pre-BiCG-STAB method, whereas the other methods do not have such a theoretical upper bound. In practice, we found that the Pre-BiCG and Pre-BiCG-STAB methods actually require much less number of iterations than  $N_d$ , even when  $N_d$  is large.

## 6. RESULTS AND DISCUSSIONS

The main purpose of this paper is to propose a new method to solve the line transfer problems in spherically symmetric media. In this section, we show some illustrative examples in order to compare with the famous benchmarks for spherical transfer solutions presented in the papers by Kunasz & Hummer (1974). In Figure 4, we show source functions for different test cases. Figure 4(a) shows the source functions for  $\epsilon = 10^{-2}$  and  $\epsilon = 10^{-4}$  for  $R = 300$ , and  $T = 10^3$ . Other model parameters are  $(\tilde{n}, \beta_c, B_v) = (2, 0, 1)$ . We use a Doppler profile to compare with the results of Kunasz & Hummer (1974). The plane parallel result is also shown for comparison. When  $\epsilon = 10^{-2}$ , we observe

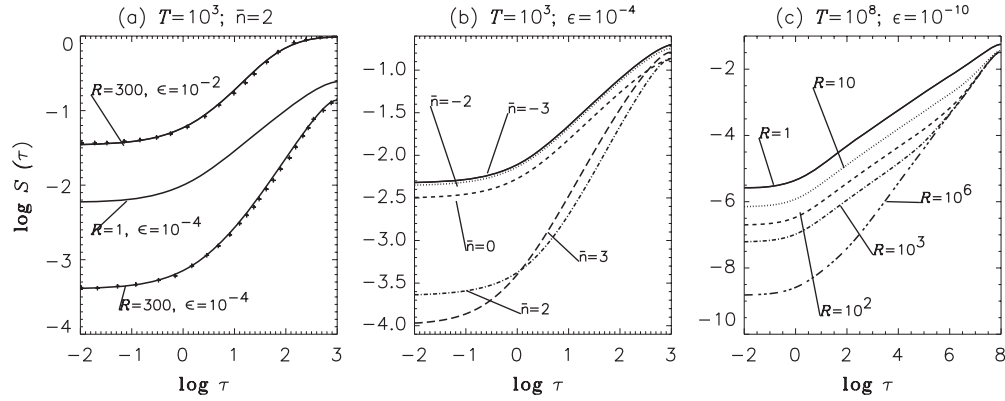


**Figure 4.** (a) Source function variation with optical depth is shown for a spherical media with inverse-square opacity variation for two different values of  $\epsilon$ . The symbols show the benchmark solution read from Kunasz & Hummer (1974), which compare well with the solution of our method (Pre-BiCG: full lines). The plane parallel solution ( $R = 1$ ) is shown for comparison. Panel (b) shows the effect of power-law opacity indices  $\bar{n}$  on the source function variation with  $\tau$ . In panel (c) the effects of spherical extension  $R$  are shown by taking a difficult case of a highly scattering, effectively optically thin medium.

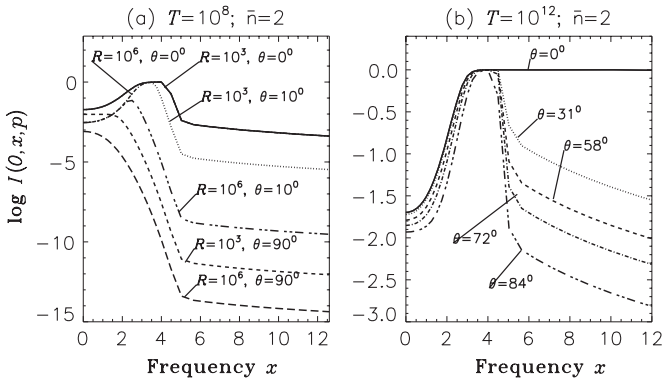


**Figure 5.** Angular dependence of emergent intensities in highly extended spherical media ( $R = 10^3$  and  $R = 10^6$ ). In panel (a), the profiles for the central ray ( $\theta = 0^\circ$ ) and the lobe rays ( $\theta = 10^\circ, 90^\circ$ ) are shown. Panel (b) shows the line profiles formed in a semi-infinite spherical atmosphere with  $R = 300$  and  $T = 10^{12}$ .

that thermalization is reached at the thermalization length for the Doppler profile namely  $1/\epsilon = 100$ . When  $\epsilon = 10^{-4}$ , thermalization does not occur. Clearly, the minimum value of the source function is  $\epsilon B_\nu$ . For the large values of  $R = 300$  and opacity index  $\bar{n} = 2$ , as  $r$  increases the opacity decreases steadily and the source function indeed approaches its minimum value near the surface layers. For this case, the departure of the source function from the planar limit is severe near the surface. It can be shown (the dashed line of Figure 4(b); see also Figure 3 of Kunasz & Hummer 1974) that this departure is not so acute when  $\bar{n} = 0$ , but is more acute when  $\bar{n} = 3$  (the dash triple-dotted line in Figure 4(b)). In Figure 4(b), we plot the source function for the same model as in Figure 4(a) but for various values of  $\bar{n}$ . For negative  $\bar{n}$ , the distinction between  $S(\tau)$  vs.  $\tau$  curves for different  $\bar{n}$  is small. For positive  $\bar{n}$ , the effects are relatively larger (see dot-dashed and long dashed curves in Figure 4(b)).

In Figure 4(c), we show source function variation for a range of spherical extensions  $R$ . We have chosen an effectively optically thin model  $(T, \epsilon) = (10^8, 10^{-10})$  because in such a medium, thermalization effects do not completely dominate over the effects of sphericity. Other parameters are the same as in Figure 4(b). Clearly, the decrease in the value of the source function throughout the atmosphere is monotonic, with an increase in the value of  $R$  from 1 to  $10^6$ .

In Figure 5, we show effects of limb darkening in spherical atmospheres for  $R = 10^3$  and  $R = 10^6$ . The other model parameters for Figure 5(a) are  $(\bar{n}, T, \epsilon, \beta_c, B_\nu) = (2, 10^8, 10^{-4}, 0, 1)$ .

A Doppler line profile is used. From this figure, we notice absorption in the line core and emission in the near line wings ( $x \approx 4$ ) for  $\theta = 0^\circ$  and  $10^\circ$ . This is the characteristic self-reversal observed in spectral lines formed in extended spherical atmospheres. The self-reversal decreases gradually as  $\theta$  increases, and finally vanishes for large values of  $\theta$ . Indeed for extreme value of  $\theta = 90^\circ$ , we observe a pure emission line.

In Figure 5(b) we show line profiles formed in a semi-infinite spherical medium. The model parameters are the same as in Figure 5(a) except for  $(R, T) = (300, 10^{12})$ . The profiles for a range of  $\theta = 0^\circ, 31^\circ, 54^\circ, 72^\circ, 84^\circ$  are shown. For the core rays ( $\theta = 0^\circ$ ) we see a pure absorption line due to thermalization of the source function. For other angles, as expected we see chromospheric-type self-reversed emission lines, formed in the lobe part of the spherical medium.

## 7. CONCLUSIONS

In this paper, we propose a robust method called the Pre-BiCG method to solve the classical problem of line transfer in spherical media. This method belongs to a class of iterative methods based on the projection techniques. We briefly present the method and the computing algorithm. We also present a transpose-free variant called the Pre-BiCG-STAB method which is more advantageous in some of its features. The Pre-BiCG and Pre-BiCG-STAB methods are validated in terms of their efficiency and accuracy, by comparing with the contemporary iterative methods such as Jacobi, GS, and SOR. To calculate the benchmark solutions we use spherical shell atmospheres. Few difficult test cases are also presented to show that Pre-BiCG and Pre-BiCG-STAB are efficient numerical methods for spherical line transfer.

L. S. Anusha thanks Han Uitenbroek, A. Asensio Ramos, and M. Sampurna for useful discussions.

## APPENDIX

### CONSTRUCTION OF THE $\hat{A}$ MATRIX AND THE PRECONDITIONER MATRIX $\hat{M}$

In the Pre-BiCG method, it is essential to compute and store the  $\hat{A}^T$  matrix. A brute forcefully numerical way of doing this is as follows. Suppose that the dimension of the  $\hat{A}$  matrix is  $N_d \times N_d$ , where  $N_d$  is the number of depth points. By sending a  $\delta$ -source function  $N_d$  times, to a formal solver subroutine,  $N_d$

columns of the  $\hat{A}$  matrix can be calculated. But this takes a large amount of CPU time especially for large values of  $N_d$ .

Instead, there is a semianalytic way of calculating the  $\hat{A}$  matrix. By substituting the  $\delta$ -source function in the expression for the intensity on a short-characteristic stencil of three points (MOP in the standard notation), we can obtain "recursive relations for intensity matrix elements  $I_{ij}(i, j, = 1, 2, \dots, N_d)$ , which can then be integrated over frequencies and angles to get the  $\hat{A}$  matrix. Finally,  $\hat{A} = [\hat{I} - (1 - \epsilon)\hat{\Lambda}]$ . The diagonal of  $\hat{\Lambda}$  is  $\hat{\Lambda}^*$  and the diagonal of  $\hat{A}$  is the preconditioner matrix  $\hat{M}$ .

For the plane parallel full-slab problem, this is given in Kunasz & Auer (1988). In radiative transfer problems with spherical symmetry, it is sufficient to compute the solution on a quadrant. However, this causes a tricky situation, in which we have to define a mid-line (see Figure 1) on which a non-zero boundary condition  $I^+ = I^-$  has to be specified. For the outgoing rays, the mid-vertical line is the starting grid point for a given ray. Since the intensity at the starting point is non-zero ( $I^+ = I^-$ ), intensity at any interior point depends on the intensity at all the previous points. Recall that

$$I_k(\mu > 0) = I_{k+1}(\mu > 0) \exp(-\Delta\tau_k(\mu > 0)) + \Psi_{k-1}S_{k-1} + \Psi_k S_k + \Psi_{k+1}S_{k+1} \quad (A1)$$

and

$$I_{k+1}(\mu > 0) = I_{k+2}(\mu > 0) \exp(-\Delta\tau_{k+1}(\mu > 0)) + \Psi_k S_k + \Psi_{k+1}S_{k+1} + \Psi_{k+2}S_{k+2}, \quad (A2)$$

and so on until we reach the mid-line. It is easy to see from above equations that intensity calculation at a short-characteristic stencil MOP is not confined only to the intensity on MOP, but also on all previous points, through spatial coupling. This is specific to performing radiative transfer on a spherical quadrant. Note that even for the construction of a diagonal  $\hat{\Lambda}$ , all the elements  $I_{ij}$  of the intensity matrix have to be computed. We present below the recursive relations to compute  $I_{ij}(i, j = 1, 2, \dots, N_d)$ .

#### For the incoming rays ( $\mu < 0$ ): Reverse sweep

DO  $i = 1, 2, \dots, N_d$

Consider an arbitrary spatial point  $i$ . The  $\delta$ -source vector is specified as

$$S(\tau_i) = 1, \quad S(\tau_j) = 0 \quad \text{for } i \neq j. \quad (A3)$$

DO  $ip = 1, 2, \dots, N_p$ , where  $N_p$  is the total number of impact parameters.

For the inner boundary points, define  $N_{v_p} = N_d$  for the core rays and  $N_{v_p} = N_d - (ip - N_c - 1)$  for lobe rays. The index  $N_{v_p}$  represents the total number of points on a given ray of the constant impact parameter  $p$ . The external boundary condition has to be taken as zero for constructing integral operators like  $\hat{\Lambda}$ :

$$I_{i1}(\tau_i, \tau_1, x, p) = 0. \quad (A4)$$

For those rays (with index  $ip$ ) for which  $p(ip) \leq r(i)$

DO  $j = 2, 3, \dots, N_{v_p}$

IF

( $j = i + 1$ ) and ( $j = N_d$  or  $p(ip) = r(j)$ ), which are interior boundary points

$$I_{i,j}(\tau_i, \tau_j, x, p) = I_{i,j-1}(\tau_i, \tau_{j-1}, x, p) \exp(-\Delta\tau_j(\mu)) + \Psi_u(j, x, p, \mu < 0) + \Psi_d(j, x, p, \mu < 0) \quad (A5)$$

This is because at these interior boundary points we assume  $S_d = S_u$  and  $S_d = S_u = 1$  when  $j = i + 1$ .

ELSE

(Non interior boundary points)

If  $j = i + 1$

$$I_{i,j}(\tau_i, \tau_j, x, p) = I_{i,j-1}(\tau_i, \tau_{j-1}, x, p) \exp(-\Delta\tau_j(\mu)) + \Psi_d(j, x, p, \mu < 0) \quad (A6)$$

Else if  $j = i$

$$I_{i,j}(\tau_i, \tau_j, x, p) = I_{i,j-1}(\tau_i, \tau_{j-1}, x, p) \exp(-\Delta\tau_j(\mu)) + \Psi_0(j, x, p, \mu < 0) \quad (A7)$$

Else if  $j = i - 1$

$$I_{i,j}(\tau_i, \tau_j, x, p) = I_{i,j-1}(\tau_i, \tau_{j-1}, x, p) \exp(-\Delta\tau_j(\mu)) + \Psi_u(j, x, p, \mu < 0) \quad (A8)$$

Else

if ( $j \leq i - 2$ )

$$I_{i,j}(\tau_i, \tau_j, x, p) = 0 \quad (A9)$$

else

$$I_{i,j}(\tau_i, \tau_j, x, p) = I_{i,j-1}(\tau_i, \tau_{j-1}, x, p) \exp(-\Delta\tau_j(\mu)) \quad (A10)$$

end if

End if

END IF

END DO

For those rays for which  $p(ip) > r(i)$

DO  $j = 2, 3, \dots, N_{v_p}$

$$I_{i,j}(\tau_i, \tau_j, x, p) = 0 \quad (A11)$$

END DO

END DO

END DO

#### For the outgoing rays ( $\mu > 0$ ): Forward sweep

DO  $i = N_d, N_d - 1, \dots, 1$

$$S(\tau_i) = 1, \quad S(\tau_j) = 0 \quad \text{for } i \neq j \quad (A12)$$

DO  $ip = 1, 2, \dots, N_p$

For  $j = N_{v_p}$  (Inner boundary point)

$$I_{i,j}(\tau_i, \tau_j, x, p) \quad (\mu > 0) = I_{i,j}(\tau_i, \tau_j, x, p) \quad (\mu < 0) \quad (A13)$$

For non-boundary points

For those rays (with index  $ip$ ) for which  $p(ip) \leq r(i)$

DO  $j = N_{v_p} - 1, N_{v_p} - 2, \dots, 1$

If  $j = i + 1$

$$I_{i,j}(\tau_i, \tau_j, x, p) = I_{i,j+1}(\tau_i, \tau_{j+1}, x, p) \exp(-\Delta\tau_j(\mu)) + \Psi_d(j, x, p, \mu > 0) \quad (A14)$$

Else if  $j = i$

$$I_{i,j}(\tau_i, \tau_j, x, p) = I_{i,j+1}(\tau_i, \tau_{j+1}, x, p) \exp(-\Delta\tau_j(\mu)) + \Psi_0(j, x, p, \mu > 0) \quad (A15)$$

Else if  $j = i - 1$

$$I_{i,j}(\tau_i, \tau_j, x, p) = I_{i,j+1}(\tau_i, \tau_{j+1}, x, p) \exp(-\Delta\tau_j(\mu)) + \Psi_u(j, x, p, \mu > 0) \quad (A16)$$

END DO

Else

$$I_{i,j}(\tau_i, \tau_j, x, p) = I_{i,j+1}(\tau_i, \tau_{j+1}, x, p) \exp(-\Delta\tau_j(\mu)) \quad (\text{A17})$$

End if

END DO

For those rays for which  $p(ip) > r(i)$ DO  $j = N_{vp}, N_{vp} - 1, \dots, 1$ 

$$I_{i,j}(\tau_i, \tau_j, x, p) = 0 \quad (\text{A18})$$

END DO

END DO

END DO

The algorithm given above saves a great deal of computing time by cutting down the number of calls to the formal solver  $-2$  instead of  $N_d$ —the first call to store  $\Psi$  and  $\Delta\tau$  at all depth points, and the second call to compute  $I_{ij}$ .

## REFERENCES

- Asensio Ramos, A., & Trujillo Bueno, J. 2006, in EAS Pub. Ser. 18, Radiative Transfer and Applications to Very Large Telescopes, ed. Ph. Stee (Les Ulis: EDP Sciences), 25
- Auer, L. H. 1984, in Methods in Radiative Transfer, ed. W. Kalkofen (Cambridge: Cambridge Univ. Press), 237
- Auer, L. H. 1991, in Stellar Atmospheres: Beyond Classical Models, ed. L. Crivellari, I. Hubeny, & D. G. Hummer (Dordrecht: Kluwer), 9
- Auer, L. H., Fabiani Bendicho, P., & Trujillo Bueno, J. 1994, A&A, **292**, 599
- Cannon, C. J. 1973, JQSRT, **13**, 627
- Chandrasekhar, S. 1934, MNRAS, **94**, 522
- Chevallier, L., Paletou, F., & Rutily, B. 2003, A&A, **411**, 221
- Daniel, F., & Cernicharo, J. 2008, A&A, **488**, 1237
- Gros, M., Crivellari, L., & Simonneau, E. 1997, ApJ, **489**, 331
- Hamann, W.-R. 1985, A&A, **145**, 443
- Hamann, W.-R. 2003, in ASP Conf. Ser. 288, Stellar Atmosphere Modeling, ed. I. Hubeny, D. Mihalas, & K. Werner (San Francisco, CA: ASP), 171
- Hestenes, M. R., & Stiefel, E. 1952, J. Res. Natl. Bur. Stand, **49**, 409
- Hubeny, I. 2003, in ASP Conf. Ser. 288, Stellar Atmosphere Modeling, ed. I. Hubeny, D. Mihalas, & K. Werner (San Francisco, CA: ASP), 17
- Hubeny, I., & Burrows, A. 2007, ApJ, **659**, 1458
- Hummer, D. G., & Rybicki, G. B. 1971, MNRAS, **152**, 1
- Klein, R. I., Castor, J. I., Greenbaum, A., Taylor, D., & Dykema, P. G. 1989, JQSRT, **41**, 199
- Kosirev, N. A. 1934, MNRAS, **94**, 430
- Kunasz, P. B., & Auer, L. H. 1988, JQSRT, **39**, 67
- Kunasz, P. B., & Hummer, D. G. 1973, MNRAS, **166**, 57
- Kunasz, P. B., & Hummer, D. G. 1974, MNRAS, **166**, 19
- Mihalas, D. 1978, Stellar Atmospheres (2nd ed.; San Francisco, CA: Freeman)
- Olson, G. L., Auer, L. H., & Buchler, J. R. 1986, JQSRT, **35**, 431
- Paletou, F., & Anterrieu. 2009, A&A, accepted (arXiv:0905.3258)
- Peraiah, A. 2002, An Introduction to Radiative Transfer (Cambridge: Cambridge Univ. Press)
- Peraiah, A., & Grant, I. P. 1973, J. Inst. Math. Appl., **12**, 75
- Saad, Y. 2000, Iterative methods for Sparse Linear Systems (2nd ed.; Philadelphia, PA: SIAM)
- Scharmer, G. B. 1981, ApJ, **249**, 720
- Schmid-Burgk, J. 1974, A&A, **32**, 73
- Trujillo Bueno, J., & Fabiani Bendicho, P. 1995, ApJ, **455**, 646
- Werner, K., & Husfeld, D. 1985, A&A, **148**, 417